# The unusual interactions between polymer grafted cellulose nanocrystal aggregates

Soft Matter

RSC Publishing

PAPER

View Article Online
View Journal | View Issue



Cite this: *Soft Matter*, 2013, **9**, 8965

# The unusual interactions between polymer grafted cellulose nanocrystal aggregates

Orlando J. Rojas,[ab] Arcot R. Lokanathan,[b] Eero Kontturi,[b] Janne Laine[b] and Henry Bock*[c]

Received 28th May 2013
Accepted 26th July 2013

DOI: 10.1039/c3sm51494c

**www.rsc.org/softmatter**

Using computer simulations we study how a corona of polymer molecules grafted to cellulose nanocrystal aggregate (CNA) particles influences the interaction between pairs of parallel CNAs. The resulting distance and orientation (face-to-face *versus* edge-to-edge) dependence is very rich and counterintuitive. Although the unperturbed polymer corona assumes cylindrical symmetry relatively quickly as the degree of polymerisation increases, the polymer mediated interactions between the grafted particles are strongly orientation dependent. Rather unexpectedly we find that the forces in the face-to-face orientation are much larger than in the edge-to-edge configuration although in the latter case the distance between the particle surfaces is much smaller. The reason for this effect is that overall the face-to-face orientation leads to larger chain confinement. Interestingly, we find that the deviations of the polymer mediated interactions from cylindrical symmetry are larger in the case of longer grafted molecules compared to shorter ones. When the distance between the CNAs becomes larger and the overlap of the polymer coronas becomes small, the orientation dependence of the mediated interaction vanishes and the particles behave as cylindrical rods. However, this is only a crossover point where the behaviour of the system inverts to slightly larger forces in the edge-to-edge compared to the face-to-face configuration. Thus, even though the polymer density around the CNAs is nearly perfectly cylindrically symmetric the polymer mediated interactions are strongly orientation dependent, revealing the polygon character of the CNA cross-section.

## 1 Introduction

The physical and geometrical properties of cellulose nanocrystals (CNC) have attracted recent interest of the research communities as new applications are discovered for these naturally occurring nanoparticles.[1,2] It is well known that CNCs have high aspect ratios (length-to-width), $L/w$ spanning a range that varies with the CNC source, between 10 for cotton and *ca.* 70 for tunicate.[1,3,4] The subject to debate, however, is the exact geometry of CNC cross-sections.

CNCs are extracted from native cellulose microfibrils *via* acid hydrolysis, which breaks the disordered regions and leaves the crystalline regions intact. Therefore, the CNC cross-section is often interpreted to resemble the cross-section of the original cellulose microfibril. Unfortunately, there is little consensus over the microfibril cross-section. Early accounts[5] suggest a rectangular shape which has been later supported by electron microscopy imaging of very large microfibrils.[6] More recently, a hexagonal cross-section has been suggested.[7,8] In addition, the validity of both the rectangular and the hexagonal model has been rightly questioned.[9] The subject of the nanocrystal – or microfibril – shape is not trivial since the cross-section impacts the type, size and orientation of the main crystal faces. This in turn is important because the different faces have very different physical–chemical properties, including hydrophobicity and hydrogen bonding ability[10,11] all of which determine how CNCs interact and interface with other materials.

The size of the microfibrils that constitute the origin of CNCs is initially determined by biosynthesis. Despite constant progress,[12] the processes that control the structure of microfibrils perpendicular to their axis remain elusive. The primary cellulose producing units, terminal protein complexes (TCs), are reported to consist of 6 × 6 cellulose synthases that could in principle produce 36 cellulose chains simultaneously,[7] but there is also evidence that the primary crystalline unit could consist of 24 cellulose chains.[9] The arrangements and geometries of the TCs also depend on their biological origin.

In the cell walls, the microfibrils are often assembled in larger structures, resulting in larger CNC structures, which are here referred to as cellulose nanocrystal aggregates. It is very often that experimental work reports CNAs in the literature rather than CNCs.[3] When considering the shape of CNAs, one

[a]*Departments of Forest Biomaterials and Chemical and Biomolecular Engineering, North Carolina State University, Raleigh, USA*

[b]*Department of Forest Products Technology, Aalto University, Espoo, Finland*

[c]*Institute of Chemical Sciences, Heriot Watt University, Edinburgh, UK. E-mail: h.bock@hw.ac.uk*

has to consider that they are prepared by hydrolysis with concentrated sulphuric acid. Taking into account that sulphuric acid even degrades the sidewalls of carbon nanotubes, it is likely that edges and corners of the CNCs and CNAs are also subjected to extensive erosion and that rearrangements may occur. Indeed, a recent study on commercial acid hydrolysed grades of cellulose reported cross-sectional shapes that were uncharacteristic for biological CNCs or CNAs.[13]

To make matters even more complicated CNCs seem to be twisted.[2,14] The direct visual proof is difficult, but more indirect evidence has existed for quite some time. The first indication of a twist came with the discovery of chiral nematic phases (*e.g.* ref. 2 and 15–17). It was proposed that the origin of the chiral phase of CNCs might be a twist of the crystal. Although many questions remain there is now compelling evidence that the twist does exist[9] and that it may originate from internal stresses. These stresses are caused by weaker hydrogen bonding on the surfaces of the crystals, especially in the case where they are broken by sulfatation or other functionalisations. This results in slightly larger intermolecular distances and stretching of the cellulose chains, which the crystal accommodates by twisting. It is unknown, however if and how this twist is inherited by the CNAs from its underlying CNCs. If the origin of the chiral nematic phases is the twist of the constituting particles, then the CNAs should be twisted too, because they are the ones most often used in experiments reporting chiral phases (*e.g.* ref. 15).

This intense debate inspires the question: are the exact shape and twist of CNAs important for their technical application? In this paper we focus on the importance of edges, *i.e.* deviations of the particle shape from cylindrical symmetry. While this study is inspired by cellulose nanocrystal aggregates, rod shaped nanocrystals with nm-sized and polygon-shaped cross-sections have also been produced from various inorganic materials.[18,19] It is also likely that the cross-section of the closely related natural chitin nanocrystals[20,21] could be polygonal.

For this discussion, it is important to consider that CNCs and CNAs are almost never used in their native state, because they are essentially insoluble in all relevant solvents. Since cellulose particles can be sourced from biomass, sustainability and environmental friendliness are great driving forces for their utilisation. In such a case water is the first-choice solvent. As CNCs and CNAs easily aggregate in water, their aqueous suspensions must be stabilised. Most commonly they are electrostatically stabilised[2,4,22] by surface charges, which are introduced, *e.g.* during sulfatation. Alternatively water-soluble polymers can be grafted to the particles.[15,23–25] The third option, used to a lesser extent, is adsorption of amphiphilic molecules, such as surfactants[26,27] or copolymers.[28]

All these methods create long-distance repulsions between the CNAs. This raises the question whether or not the underlying non-cylindrical shape of the particles matters for these interactions or if the particles effectively become cylindrical rods. Here we focus on the interactions caused by grafted polymers. They are particularly interesting as their interaction range can ultimately be limited by the length of the grafted molecules.[29] As the length scale of the steric repulsion, which is of the order of the size of the grafted chains, is well in the range of the small dimensions of CNCs and CNAs, an interesting interplay between these length scales is expected.

Here we report on mesoscale computer simulations to investigate the interplay between the cross-sectional geometry of the CNAs and the length of the grafted molecules. Similar to brushes grafted on patterned planar surfaces[30,31] the polymer brushes grafted to the CNA faces must be expected to "spill over" at the edges. This should smooth out any non-cylindrical features and eventually result in a cylindrical polymer corona. While we find that this is indeed the case, the polymer mediated forces between the grafted CNAs are strongly orientation dependent.

Our results indicate that the edges of CNCs and CNAs play important roles in the interparticle interactions. This must be expected to affect their self- or directed-assembly. Such effects are relevant in coating and structuring with CNCs/CNAs. It is also relevant to the association behaviour of CNCs and thus affects the rheology, dispersion and other phenomena relevant to the application of CNCs/CNAs. This contribution intends for the first time to reveal such aspects that are otherwise elusive to experimentation.

## 2 Model and simulation

Since the exact shape of CNAs is quite elusive and varies between different cellulose-producing species, we focus on fundamental aspects, in particular the existence of edges along the particle surface, while foregoing other details such as the specific surface chemistry.

Because of the detailed insight computer simulations provide, they are very well suited and widely used to study grafted polymers.[32,33] Here the grafted polymer molecules are represented by chains of beads. Beads $k$ and $l$, which are nearest neighbours in the same chain, are bonded *via* a harmonic bond potential

$$\phi_{\mathrm{bond}}(r_{kl}) = \varepsilon_{\mathrm{bond}}(r_{kl} - r_{\mathrm{bond}})^2, \tag{1}$$

where $\varepsilon_{\mathrm{bond}}$ is the depth of the potential well, $r_{\mathrm{bond}}$ is the bond length, $r_{kl} = ||\mathbf{r}_{kl}||$, $\mathbf{r}_{kl} = \mathbf{r}_k - \mathbf{r}_l$ and $\mathbf{r}_k$ and $\mathbf{r}_l$ are the positions of $k$ and $l$, respectively.

The solvent, water, is treated implicitly and the grafted polymer is assumed to be soluble. This situation can be modelled by polymer beads interacting with each other *via* the repulsive Weeks–Chandler–Andersen (WCA) potential $\phi(r_{ij})$.

$$\phi_{\mathrm{LJ}}(r_{ij}) = 4\varepsilon\left[\left(\frac{\sigma}{r_{ij}}\right)^{12} - \left(\frac{\sigma}{r_{ij}}\right)^{6}\right], \tag{2}$$

$$\phi(r_{ij}) = \begin{cases} \phi_{\mathrm{LJ}}(r_{ij}) - \phi_{\mathrm{LJ}}(r_{\mathrm{cut}}) & r_{ij} < r_{\mathrm{cut}} \\ 0 & r_{ij} \geq r_{\mathrm{cut}} \end{cases}, \tag{3}$$

where $r_{\mathrm{cut}} = 2^{1/6}$ is the cut-off-radius, $\varepsilon$ is the well depth and $\sigma$ is the length parameter of the Lennard-Jones (LJ)(12,6) potential in 2.

Grafting is modelled by placing anchor beads at random positions along the surface of the crystal at a fixed distance from the surface that coincides with the minimum of the CNA/polymer interaction. During the simulation the anchor beads are

 

not allowed to move, but they interact with all other polymer beads. Initially the polymer chains are grown as almost straight chains perpendicular to the surfaces. The slight randomness of the bead positions aids the initial equilibration.

Initially the CNAs are placed far enough apart to avoid overlap of polymer chains grafted to different CNAs. Then the system is relaxed, after which the particles are slowly moved to a given distance. Then the system is fully equilibrated before results are determined.

While the model is very simple it seems important to choose a sensible grafting density. One common method to graft polymers to CNAs is to first react some of the hydroxyl groups with sulphuric acid to form sulphate esters. Then a polymer chain with a cationic terminal functionality is attached *via* a strong ionic interaction. To obtain a rough estimate of the grafting density we assume that a polymer chain is attached to each sulphate ester group. Then the grafting density can be estimated from the efficiency of the sulphate ester formation. In ref. 34 this is estimated to be 0.62% of all hydroxyl functions of the CNAs leading to a grafting density of $\approx 0.3$ nm$^{-2}$.

To translate this grafting density into the model, a physical length scale needs to be chosen, *i.e.* a value for the length parameter $\sigma$ needs to be chosen. If $\sigma = 1$ nm then the model grafting density is $0.3\sigma^{-2}$. The choice of $\sigma = 1$ nm is sensible because it is similar to the Kuhn length of typical polymers, such as poly ethylene-oxide.†

The exact cross-section of CNCs and CNAs is intensely debated as pointed out in the introduction. However, in all possible geometries well defined crystal faces are connected by edges rendering the particles non-cylindrical. Here we focus on the existence of these edges, which can be modelled by representing the CNAs as quadratic prisms. Their aspect ratio is usually large, which suggests their treatment as infinite in the long dimension. This eliminates any effects from edges and corners at both ends, which is sensible considering that these regions are comparatively small and even less well understood than the cross-section.

The simplest way to represent such a crystal is to view it as continuum matter assuming that the internal structure of the CNAs is not relevant for the grafted polymers. The interaction with the polymer beads is then found by integration over the CNA's volume. Such a procedure makes it possible to represent the edges of the crystal well. We do this numerically by placing beads representing the solid on a simple cubic lattice and then sum over all positions. The solid beads are assumed to have the same size as the polymer beads and interact with them *via* the Lennard-Jones (LJ)(12,6) potential in eqn (2). Since the summation is quite costly, we calculate a fine 2D grid of the potential before the simulation. During the simulation the interaction between the polymer beads and the crystal is determined by bilinear interpolation between the four nearest grid points.

Unfortunately, it is largely unknown how different polymers interact with CNAs. Clearly, this would depend on the polymer, which crystal faces are exposed and what their specific properties are. However, in this study we focus on the influence of the CNAs shape on the grafted polymers. Therefore the interactions between the CNAs and the chains anchored (grafted) on them are chosen to be repulsive with only a minimal attraction at short distances (Table 1). The potential is represented in Fig. 1.

The system is simulated using standard Dissipative Particle Dynamics (DPD). In addition to the conservative forces discussed above, DPD requires random forces

$$F_{ij}^{\mathrm{R}} = \begin{cases} -\xi\omega^{\mathrm{R}}(r_{ij})\theta_{ij}\hat{\mathbf{r}}_{ij} & r_{ij} \le r_{\mathrm{c}} \\ 0 & r_{ij} > r_{\mathrm{c}} \end{cases} \quad (4)$$

and dissipative forces

$$F_{ij}^{\mathrm{D}} = \begin{cases} -\gamma\omega^{\mathrm{D}}(r_{ij})(\hat{\mathbf{r}}_{ij}\cdot\mathbf{v}_{ij})\hat{\mathbf{r}}_{ij} & r_{ij} \le r_{\mathrm{c}} \\ 0 & r_{ij} > r_{\mathrm{c}} \end{cases} \quad (5)$$

**Table 1** Model and simulation parameters in reduced units

| | |
|---|---|
| **Grafted polymer chains** | |
| Number of beads = 8, 22 | Grafting density = 0.3 |
| $\varepsilon = 1.0$ | $\sigma = 1.0$ |
| $\varepsilon_{\mathrm{bond}} = 4.0$ | $\sigma_{\mathrm{bond}} = 1.2$ |
| **Cellulose nanocrystals** | |
| Side length of quadratic cross-section = 13.0 | Distance between centres, $d$ = 16.0–68.0 |
| Length = infinite | |
| $\varepsilon_{\mathrm{CNA}} = 1.2\ell^3$ | $\sigma_{\mathrm{CNA}} = 1.0$ |
| Lattice parameter (simple cubic), $\ell = 0.25$ | Cutoff for integration along the CNA = 10.0 |
| Mesh size of potential grid (square) = 0.1 | |
| **Simulation** | |
| $T = 0.7$ | $\Delta t = 0.01$ |
| Cut-off non-conservative, $r_{\mathrm{c}} = 2.5$ | $\xi = 1.0$ |
| Last equilibration = $1.10^5\Delta t$ | Production = $30 \times 10^6\Delta t$ |

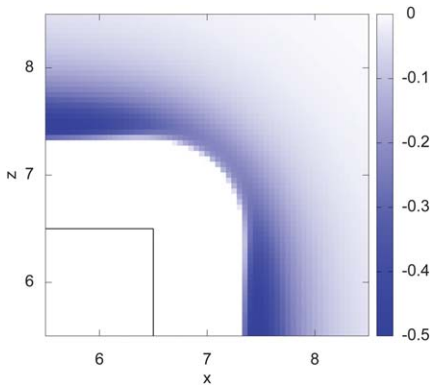


**Fig. 1** The interaction potential between the polymer beads and the nanocrystal as a colour map. The scale is given in the figure. Shown is only one quadrant. The white area in the bottom left corner represents the nanocrystal. The position of the surface layer of beads constituting the nanocrystal is indicated by black lines and will be used in all following plots to indicate the nanocrystal. Clearly visible is the lower attraction near the edge. The edge is slightly rounded because the solid is built from beads of finite size.

† Note that although the chains are fully flexible, the bead–bead distance in the present model is not exactly equal to its Kuhn length because it has some self-avoidance.

where $\hat{\mathbf{r}}_{ij} = \mathbf{r}_{ij}/||\mathbf{r}_{ij}||$, $\theta_{ij}$ is a random variable with limits −1 and 1, and zero mean (see ref. 35 for the utilized random number generator), $\xi$ and $\omega^{\mathrm{R}}(r_{ij})$ are the strength parameter and the weight function of the random force, $\gamma$ and $\omega^{\mathrm{D}}(r_{ij})$ are the strength parameter and the weight function of the dissipative force, $\mathbf{v}_{ij} = \mathbf{v}_j - \mathbf{v}_i$, $\mathbf{v}_i$ is the velocity of bead $i$ and $r_c = 2.5\sigma$ is the cut-off of the dissipative and the random force.

The method allows the simulation of a canonical ensemble. In the canonical ensemble the dissipative and the random forces are connected by the fluctuation dissipation theorem leading to

$$\omega^{\mathrm{D}}(r_{ij}) = [\omega^{\mathrm{R}}(r_{ij})]^2,\ \xi^2 = 2\gamma k_{\mathrm{B}}T, \tag{6}$$

where $k_{\mathrm{B}}$ is Boltzmann's constant and $T$ is the temperature that can be freely chosen. Thus, the random and the dissipative forces together constitute the DPD thermostat. Here we use the weight functions originally published in ref. 36.

$$\omega^{\mathrm{D}}(r_{ij}) = \begin{cases} (1 - r_{ij}/r_c)^2, & r_{ij} \le r_c \\ 0 & r_{ij} > r_c \end{cases} \tag{7}$$

It is important to recognise that $F_{ij}^{\mathrm{R}}$ is a stochastic force which requires slight modifications of the integration algorithm.[36] All model and simulation parameters are given in Table 1.

For simplicity we employ the customary reduced quantities: lengths are given in units of the LJ length parameter $\sigma$, the energy is scaled with the well depth of the bead/bead LJ interaction $\varepsilon$, the temperature scale is given in terms of $\varepsilon/k_{\mathrm{B}}$ and time is represented in units of $\sqrt{m\sigma^2/\varepsilon}$, where $m$ is the mass of a bead.

## 3 Shape of the grafted polymer shell

The local densities in Fig. 2 visualise the shape of the polymeric shell around the CNAs for two different polymers: 8 beads long and 22 beads long. The densities are averaged along the axis of the CNA since no structural variations are expected in this direction. The short 8-bead chains lead to a polymer layer that still resembles the square cross-section of the CNA. While the local density is affected by the shape of the CNA, it is immediately obvious that the memory of this shape is more and more lost the further one moves away from the surface. In the case of the 22-bead chains most of the density appears to have circular symmetry except for the inner most region close to the CNA's surface. We also observe some degree of layering near the CNA faces that is much weaker along the edges (see below). Such packing effects are typical for bead spring-models grafted to flat surfaces[37,38] and spherical particles[39,40] and can also be observed in hard-sphere fluids near soft repulsive walls.[41]

Bulk polymer chains are known to follow scaling laws that are identical to those of self-avoiding random walks. This indicates that flexible polymer molecules lose any memory of their chain orientation rather quickly. Extrapolating this to polymers grafted to irregular particles, one would expect that the polymer layer becomes more and more spherical the further the polymer corona extends from the particle. Indeed this has been observed in simulations of polymer grafted nanocrystals.[42] Experimentally it was found that polymer brushes grafted on small gold particles (which are non-spherical) are shorter compared to brushes of the same molecules grafted to planar surfaces, which means that the molecules also fill the space over the edges and corners.[43] A similar lateral "spillover" has been observed for laterally finite brushes on flat surfaces.[30,31] This suggests that in the present case the polymer corona around the infinitely long CNAs, modelled by square prisms, should assume cylindrical symmetry.

To investigate to which extent the grafted layer deviates from cylindrical symmetry, *i.e.*, retains a memory of the geometry of the nanoparticle it is grafted to, we follow concentric circles of

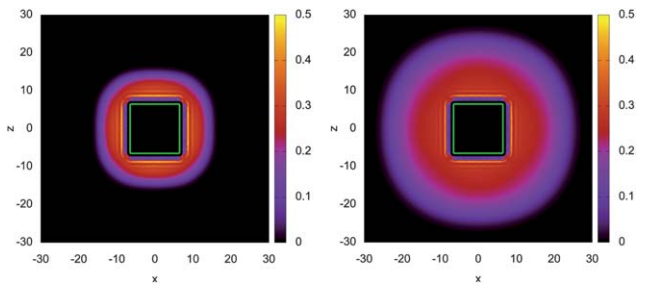


**Fig. 2** Local densities of beads of the grafted molecules in the plane perpendicular to the long axis of the CNA as a colour map (as indicated in the figure) for molecules with 8 beads (left) and 22 beads (right). The green square indicates the nanocrystal.

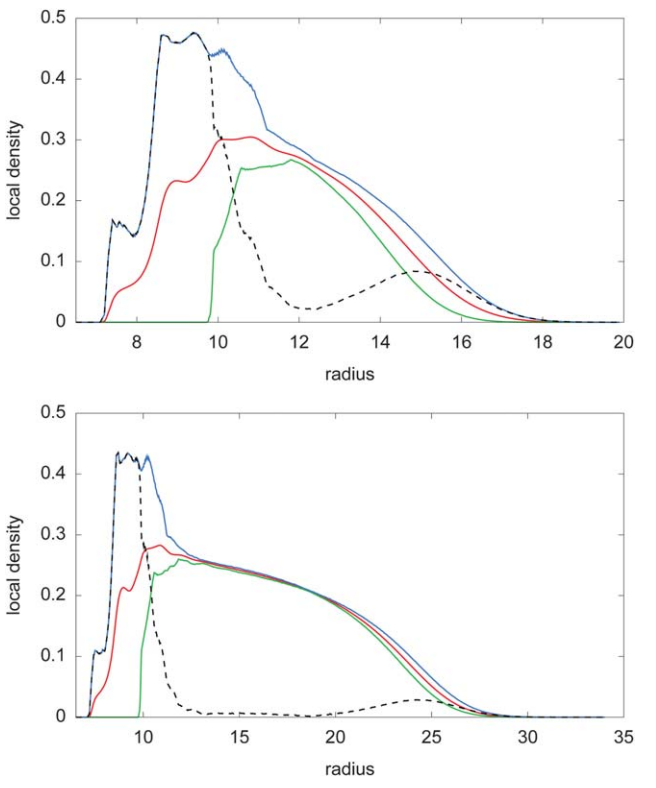


**Fig. 3** Minima (green), average (red) and maxima (blue) in the local density along concentric circles around the long axis of the crystals as a function of the circle radius to visualise deviations in the local density from cylindrical symmetry: upper panel 8-bead chains and bottom panel 22-bead chains. The dashed black curve represents the absolute difference between maximal and minimal densities.

radius $r$ around the axis of the CNA and determine extrema in the local density and its average. The results are shown in Fig. 3. Initial differences between the curves are expected due to the geometry of the CNAs and the layering. After this initial region all three curves converge for the 22-bead chains. It is quite intriguing that after a large region of cylindrical symmetry spanning from $r \approx 12$ to 20 the density starts to deviate from cylindrical symmetry again. The 8-bead chains follow the same tendency but seem to be too short to have a region of cylindrical symmetry.

This result becomes even more surprising when we determine the location of the extrema (Fig. 4). In the inner region we observe effects of the quadratic cross-section of the CNA and of layering. It is important not to misinterpret this as a local density, instead the dots indicate the location of extrema along concentric circles. Beyond this initial region maxima are located in front of the crystal faces, while along the edges the density is minimal. This is an expected curvature effect – there is more space along the edges and it grows as one moves further away from the nanocrystal. However, the differences between the maximal and minimal local density values are very small.

All the more intriguing is therefore the inversion of the positions of the extrema as one moves further out (Fig. 4). The differences in the density (Fig. 3) might appear small, but have a noticeable impact on the interaction between polymer grafted CNAs as we show below.

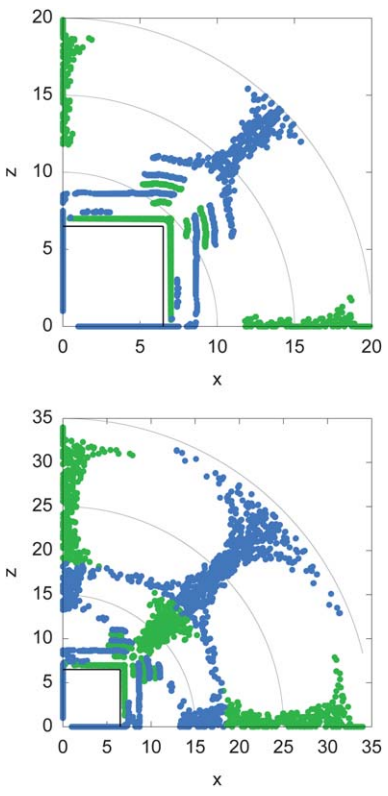


**Fig. 4** Location of local density minima (green) and maxima (blue) along concentric circles around the long axis of the crystals. The circular arches in grey are included to guide the eye. The mirror symmetry along the diagonal has been used to mirror all points. Upper panel 8-bead chains and bottom panel 22-bead chains. Apparent is the location of density maxima along the edges in the outer regions.

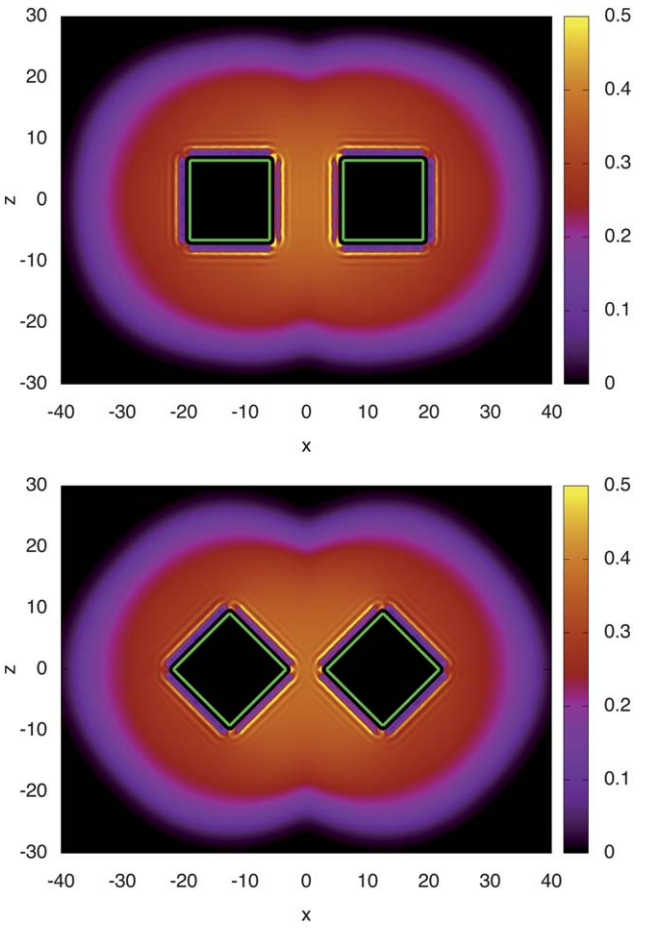


**Fig. 5** Local densities to visualize the face-to-face (top) and the edge-to-edge (bottom) configuration. Visible is also the higher local density between the CNAs. In green indicated are the CNAs and the colour code for the density is given in the figure.

These results suggest that the most important and most interesting configurations for a pair of grafted nanocrystals are the face-to-face and the edge-to-edge configuration (Fig. 5). Density profiles for these two directions, *i.e.* perpendicular to the face and diagonal (45° to the previous), are plotted in Fig. 6. Near the crystal faces we observe weak oscillations in the density. It is interesting that the highest peak is not located in the very weak minimum of the crystal/bead interaction, instead this is the location of the very low first maximum in the density. It appears that the ordering is due to the grafting, *i.e.* the bonding between the first chain bead and the immobile anchor bead that is placed in the potential minimum. It also appears that the chains are pulling on the anchor-beads, possibly because the lateral confinement by other grafted molecules causes configurational entropy penalties. This seems to lead to some preferential orientation of the first few segments of the chains perpendicular to the surface. The preferential orientation creates some bead/bead, bead/anchor-bead and consequently, bead/surface correlations, which are reflected in the density profile. The oscillations decay quickly as, except for the bonds, there are no bead/bead attractions. In the diagonal direction remnants of the first two oscillations (the wall peak and the highest maximum) are also visible.

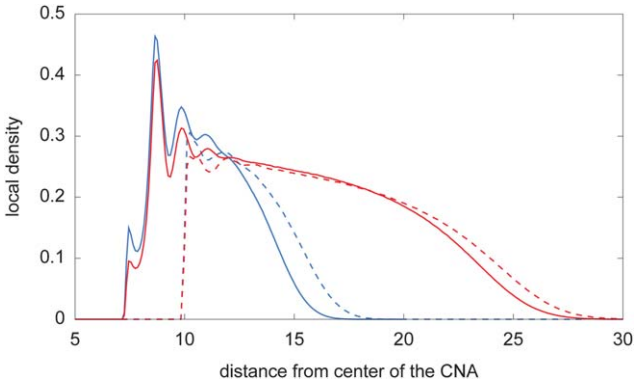


**Fig. 6** Local density profiles as a function of the distance from the centre of the CNA. Solid lines are used to show the profile perpendicular to the crystal face at the centre of the face, while dashed lines are used for the diagonal direction. Blue indicates chains with 8 beads and red indicates chains with 22 beads. The densities indicate some ordering near the surfaces and a large region of cylindrical symmetry in the 22-bead case.

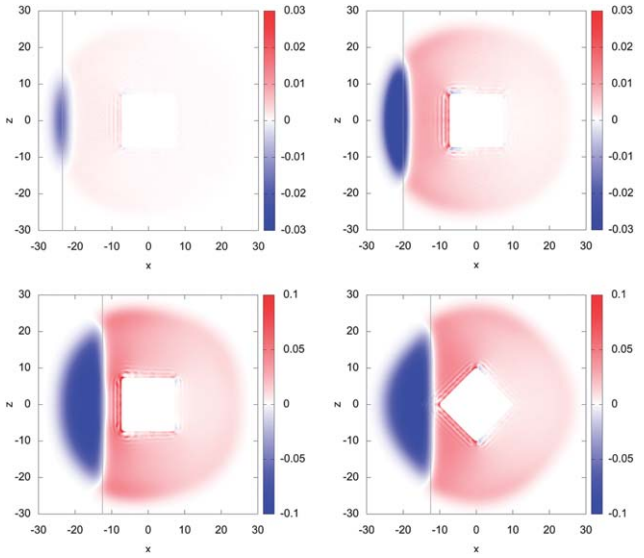


**Fig. 7** Interaction-induced deformation of the polymer coronas of pairs of CNAs as the difference between the local density of the deformed system and an undisturbed local density (as shown in Fig. 2) presented as colormaps. Red indicates the density increase and blue indicates the density decrease. The colour scales are given in the figure. Note that the colour scale for parts (c) and (d) are larger compared to parts (a) and (b). Note also that only the molecules grafted to one CNA are used for the comparison. Face-to-face configurations for three different distances, (a) 47, (b) 40 and (c) 25, and one edge-to-edge conformation at a CNA/CNA distance of 25 are compared. The grey lines indicate the centre between the CNAs. The plots reflect the increasing deformation with decreasing distance and the greater confinement in the face-to-face arrangement compared to the edge-to-edge configuration.

From this point on all densities decay monotonously. The decay is steep for the 8-bead molecules, but more gentle for the 22-bead chains. The density profiles for the 8-bead molecules clearly show that the polymeric corona is not yet cylindrical. The density profile of the 22-bead molecules has a very large region over which the density has perfect cylindrical symmetry. However, as discussed above, in the outer regions deviations occur with the density in the diagonal direction reaching out further compared to the perpendicular direction. It is interesting that near the particle surface the local density is lower in the case of the longer molecules. This would be consistent with the suggested pulling.

## 4 Grafted polymer-mediated interactions between the CNAs

The key focus of this study is to determine whether or not the grafted CNAs behave as cylindrical rods or if their behaviour reflects aspects of the geometry of the CNAs' cross-section. While the local densities indicate nearly cylindrical symmetry, it is the mutual interactions of grafted CNAs that will determine their behaviour. Here these interactions are steric repulsions originating from the overlap of the polymer coronas of pairs of grafted CNAs.

This overlap causes deformation of the polymer layer. In Fig. 7 the deformation is visualised by plotting the difference between the deformed and an unperturbed polymer corona. As expected, this difference increases with decreasing distance between the CNAs. While deformations are largest near the contact between the two coronas, it is interesting that the entire polymer coating is affected. The importance of deformation has also been observed for simulated atomic force microscopy on structured polymer brushes.[31]

Any deformation of the unperturbed polymer corona leads to a restoring force. This force should be expected to be stronger for stronger deformations. In Fig. 8 the steric repulsion forces are presented for both chain lengths considered here, namely, 8 and 22 beads in the face-to-face configuration and the edge-to-edge configuration. Because we consider the CNAs to be infinitely long we report the force per unit length, *i.e.*, the force per $1\sigma$ of CNAs. As expected from the monotonously increasing deformation, all forces increase monotonously with decreasing distance between the CNAs.

The forces are shorter ranged but increase faster with decreasing distance for the CNAs modified with the shorter grafts. The steeper increase in the force is plausible because the local density also increases faster for the shorter molecule (Fig. 6). This steeper increase of the local density leads to stronger deformation at the same overlap in the case of the shorter molecules compared to the longer ones.

This argument is interesting as it also predicts a higher force for the edge-to-edge conformation compared to the face-to-face conformation. Indeed, this is found for both molecules and small overlaps (insets in Fig. 8). It has to be noted, however, that this difference in the force is very small.

As the distance between the CNAs is decreased the face-to-face and edge-to-edge force curves cross and the behaviour is inverted. Now the repulsion in the edge-to-edge conformation is weaker compared to the face-to-face arrangement. Comparing the deformations plotted in Fig. 7(c) and (d) it is immediately obvious that in the edge-to-edge configuration the chains are deformed but not very confined. This is dramatically different in the face-to-face arrangement, where the chains grafted onto the CNA face pointing towards the other crystal are strongly confined between the opposing faces. Similar effects have been observed and

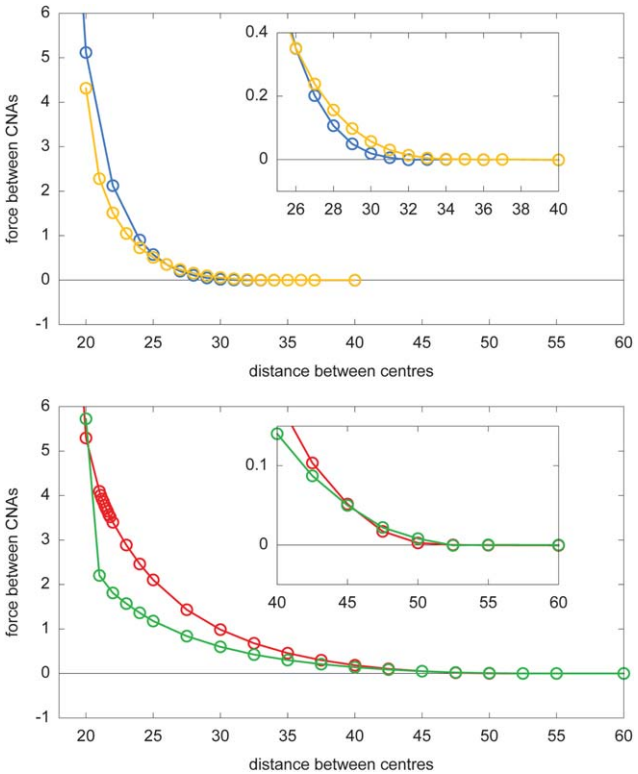


**Fig. 8** Force per unit length of nanocrystal generated by steric repulsion between grafted molecules of 8 bead length (top) and 22 bead length (bottom) as a function of the distance between the CNA centres. The face-to-face conformation (blue and red) and the edge-to-edge conformation (yellow and green) are compared. In both cases a crossover from stronger edge-to-edge forces to stronger face-to-face forces can be observed.

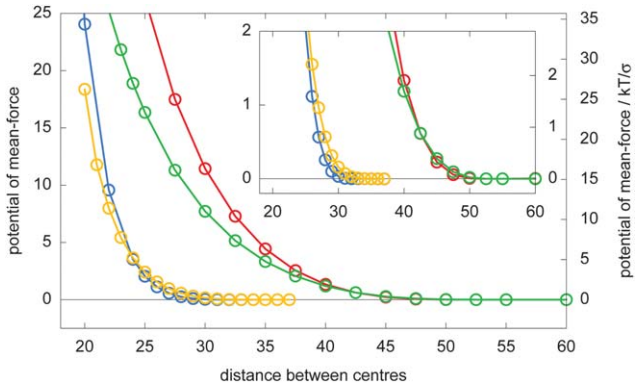


**Fig. 9** Potential of mean-force per unit length as a function of CNA/CNA distance. The colour code is the same as in Fig. 8. Clearly visible are the amplified deviations from cylindrical symmetry in the case of the longer molecules.

studied in detail for polymer brushes grafted to spherical particles by Binder *et al.* in a series of publications (see ref. 39, 40 and references therein).

At very small distances in the face-to-face cases the forces increase dramatically. Both length of grafted molecules lead to nearly identical forces which can be expected because at small distances the non-grafted ends of the molecule are squeezed out of the gap between the crystals and therefore, the region between the opposing faces must be expected to be very similar in both cases. Interestingly, there is no sign of force oscillations that are normally associated with layering (Fig. 5). However, this is consistent with our assumption of a preferential perpendicular orientation of molecule segments near the anchor bead through pulling by the rest of the molecule. Under strong confinement the molecules can no longer pull perpendicularly to the surfaces and consequently, the layering disappears.

The forces for the edge-to-edge configuration increase steeply in the same region because the layers of anchor-beads get very close. The resulting indication of cylindrical symmetry is purely coincidental and will not occur for other CNA geometries. Moreover, the forces and energies required to reach these small distances are very large and are unlikely to play a role in any application.

In Fig. 9 the potential of mean-force (PMF) is shown. As in the case of the force the PMF presented here is the PMF per $1\sigma$ of CNA. The PMF is equal to the work required to overcome the repulsive interactions (from an infinite distance).

Alternative to the interpretation presented for the forces, *i.e.* comparing the strength of the force at equal distances between the particles, we could ask how close two particles can come to each other at a given "collision" energy, *i.e.* PMF. This alternative interpretation reveals the apparent shape of the grafted CNAs.

In the case of the shorter 8-bead chain the PMFs for the face-to-face and the edge-to-edge configuration are nearly identical. Thus, the apparent shape is that of a cylinder. This is surprising as the local density is clearly non-cylindrical (Fig. 3). The reason for this behaviour is largely related to the steepness of the density profiles (Fig. 6) and consequently, of the forces (Fig. 8) and also to the aforementioned geometrical coincidence.

In the case of the longer grafted molecules we observe that at small interaction energies ($\lesssim 1kT/\sigma$) the grafted CNAs are slightly larger in the edge-to-edge configuration compared to the face-to-face configuration. This relationship is inverted for larger interaction energies ($\gtrsim 5kT/\sigma$); now the grafted crystals are larger in the face-to-face configuration compared to the edge-to-edge arrangement. This is exactly opposite of what one would expect for the ungrafted particles. The difference can be large, up to $\approx 4\sigma$ at $30kT/\sigma$. Thus, the longer molecules amplify the differences between the face-to-face and the edge-to-edge conformation.

Which forces or energies between the grafted CNAs are relevant depends on the situation and is hard to estimate. In a stable dispersion an upper limit of these interaction energies can be extracted from the energy barriers required to prevent aggregation. If aggregation is prevented, then no particle in the system has an energy higher than the barrier. For electrostatically stabilised CNCs treated as cylinders with a radius of 2 nm the required barrier was estimated to be around $5kT$.[22] This is very low and assuming that the grafted CNAs have similar energies, it would mean that the two polymeric coronas barely touch each other even for very short particles. However, in dense systems such as deposited films, the forces pushing the CNAs together might be significantly higher.

## 5 Conclusions

We have used dissipative particle dynamics simulations of chain-of-beads models to investigate if the polygonal character of the cross-section of cellulose nanocrystal aggregates is inherited by the corona of grafted polymer molecules and possibly also by the polymer mediated interactions between the grafted particles. While this work is inspired by cellulose nanocrystals, our results are relevant also for other nanocrystals with polygon cross-section.

We find that the local density of the polymer corona around isolated CNAs assumes cylindrical symmetry already at small distances from the particle surface. Thus, even grafting with relatively short molecules smoothed out the non-cylindrical surface fairly effectively. Interestingly, we observe a small but systematic deviation from this behaviour in the outermost reaches of the polymer corona. Here the local density of the polymer is slightly higher along the edges of the CNAs compared to other directions even though the inner region is already cylindrically symmetric. Except for this small deviation the grafted particles "look" essentially like cylindrical rods, *i.e.* their outer structure is essentially cylindrically symmetric.

However, the polymer mediated forces behave very differently. For most interparticle distances they are strongly orientation dependent. Rather unexpectedly we find that at the same centre-to-centre distance the forces in the face-to-face orientation are much larger than in the edge-to-edge configuration although in the latter case the distance between the particle surfaces is smaller. This is a strong effect and it means that under the same compression the grafted particles can come closer in the edge-to-edge orientation compared to the face-to-face orientation. This is opposite to the behaviour of the pristine particles. The reason for this effect is that overall the face-to-face orientation leads to larger chain confinement. This affects longer molecules stronger than shorter ones and therefore, we find that deviations from cylindrical symmetry are stronger for the longer molecules.

At larger distances between the grafted particles, where the overlap of the polymer coronas becomes small, the behaviour of the system changes to what one would expect from the unperturbed polymer densities. Here we find slightly higher forces in the edge-to-edge compared to the face-to-face arrangement, which is consistent with the slightly higher local polymer density along the edges in the outermost region of the polymer corona. This behaviour of the force is exactly opposite to what we find at shorter interparticle distances. As this crossover suggests, we also find a small region where the forces in the two orientations are the same.

In summary, at large forces between the particles the edge-to-edge orientation generates the least resistance, while at small forces the face-to-face orientation is favourable. Between these two situations is a crossover point. Around this point the particles behave essentially as cylindrical rods.

These effects elucidated using simple models suggest that the non-cylindrical symmetry of CNAs and other nanoparticles has important implications on the interactions between their grafted polymer coronas. This is consistent with the experimental observation of chiral nematic phases (*e.g.* ref. 2 and 15–17), which cannot be created by cylindrical rods. Of course, in chiral nematic phases the CNAs are not perfectly aligned which leads to more complex behaviour compared to that revealed in our study, but our results already demonstrate that the non-cylindrical structure of the CNAs "transpires" through the polymer corona. Our results are particularly important for applications exploiting densely packed and possibly aligned CNAs as in thin films where deformations of the polymer corona are expected to be large (*e.g.* ref. 16, 17 and 44–48). The interactions with planar surfaces in these cases are particularly interesting because they lead to larger chain confinement than in any CNA/CNA interaction.

## References

1 Y. Habibi, L. A. Lucia and O. J. Rojas, *Chem. Rev.*, 2010, **110**, 3479–3500.
2 S. J. Eichhorn, *Soft Matter*, 2011, **7**, 303–315.
3 S. Elazzouzi-Hafraoui, Y. Nishiyama, J.-L. Putaux, L. Heux, F. Dubreuil and C. Rochas, *Biomacromolecules*, 2008, **9**, 57–65.
4 S. Beck-Candanedo, M. Roman and D. G. Gray, *Biomacromolecules*, 2005, **6**, 1048–1054.
5 I. Ohad and D. Danon, *J. Cell Biol.*, 1964, **22**, 302–305.
6 J. Sugiyama, H. Harada, Y. Fujiyoshi and N. Uyeda, *Planta*, 1985, **166**, 161–168.
7 S.-Y. Ding and M. E. Himmel, *J. Agric. Food Chem.*, 2006, **54**, 597–606.
8 Y.-S. Liu, J. O. Baker, Y. Zeng, M. E. Himmel, T. Haas and S.-Y. Ding, *J. Biol. Chem.*, 2011, **286**, 11195–11201.
9 A. N. Fernandes, L. H. Thomas, C. M. Altaner, P. Callow, V. T. Forsyth, D. C. Apperley, C. J. Kennedy and M. C. Jarvis, *Proc. Natl. Acad. Sci. U. S. A.*, 2011, **108**, E1195–E1203.
10 B. Medronho, A. Romano, M. Miguel, L. Stigsson and B. Lindman, *Cellulose*, 2012, **19**, 581–587.
11 W. G. Glasser, R. H. Atalla, J. Blackwell, J. Malcolm Brown, R. W. Burchard, A. French, D. Klemm and Y. Nishiyama, *Cellulose*, 2012, **19**, 589–598.
12 A. Carroll, N. Mansoori, S. Li, L. Lei, S. Vernhettes, R. G. Visser, C. Somerville, Y. Gu and L. M. Trindade, *Plant Physiol.*, 2012, **160**, 726–737.
13 K. Leppänen, S. Andersson, M. Torkkeli, M. Knaapila, N. Kotelnikova and R. Serimaa, *Cellulose*, 2009, **16**, 999–1015.
14 S. Hanley, J. Revol, L. Godbout and D. Gray, *Cellulose*, 1997, **4**, 209–220.
15 J. Araki, M. Wada and S. Kuga, *Langmuir*, 2001, **17**, 21–27.
16 E. Kontturi, L.-S. Johansson, K. S. Kontturi, P. Ahonen, P. C. Thüne and J. Laine, *Langmuir*, 2007, **23**, 9674–9680.
17 J. Majoinen, E. Kontturi, O. Ikkala and D. Gray, *Cellulose*, 2012, **19**, 1599–1605.
18 S. Zeng, G. Ren, C. Xu and Q. Yang, *CrystEngComm*, 2011, **13**, 1384–1390.
19 K. Critchley, B. P. Khanal, M. L. Gorzny, L. Vigderman, S. D. Evans, E. R. Zubarev and N. A. Kotov, *Adv. Mater.*, 2010, **22**, 2338–2342.

 

20 N. Lin, J. Huang and A. Dufresne, *Nanoscale*, 2012, **4**, 3274–3294.
21 J.-B. Zeng, Y.-S. He, S.-L. Li and Y.-Z. Wang, *Biomacromolecules*, 2012, **13**, 1–11.
22 A. B. Fall, S. B. Lindström, O. Sundman, L. Ödberg and L. Wågberg, *Langmuir*, 2011, **27**, 11332–11338.
23 E. Kloser and D. G. Gray, *Langmuir*, 2010, **26**, 13450–13456.
24 J. O. Zoppe, Y. Habibi, O. J. Rojas, R. A. Venditti, L.-S. Johansson, K. Efimenko, M. Österberg and J. Laine, *Biomacromolecules*, 2010, **11**, 2683–2691.
25 J. O. Zoppe, M. Österberg, R. A. Venditti, J. Laine and O. J. Rojas, *Biomacromolecules*, 2011, **12**, 2788–2796.
26 C. Bonini, L. Heux, J.-Y. Cavaillé, P. Lindner, C. Dewhurst and P. Terech, *Langmuir*, 2002, **18**, 3311–3314.
27 D. Bondeson and K. Oksman, *Compos. Interfaces*, 2007, **14**, 617–630.
28 Q. Zhou, H. Brumer and T. T. Teeri, *Macromolecules*, 2009, **42**, 5430–5432.
29 S. Ullrich, S. P. Scheeler, C. Pacholski, J. P. Spatz and S. Kudera, *Part. Part. Syst. Charact.*, 2013, **30**, 102–108.
30 M. Patra and P. Linse, *Nano Lett.*, 2006, **6**, 133–137.
31 M. Patra and P. Linse, *Macromolecules*, 2006, **39**, 4540–4546.
32 K. Binder and A. Milchev, *J. Polym. Sci., Part B: Polym. Phys.*, 2012, **50**, 1515–1555.
33 M. Tagliazucchi and I. Szleifer, *Soft Matter*, 2012, **8**, 7292–7305.
34 Y. Li and A. J. Ragauskas, in *Cellulose Nano Whiskers as a Reinforcing Filler in Polyurethanes, Advances in Diverse Industrial Applications of Nanocomposites*, ed. B. Reddy, InTech, http://www.intechopen.com/books/advances-in-diverse-industrial-applications-of-nanocomposites/cellulose-nano-whiskers-as-a-reinforcing-filler-in-polyurethanes, 2011.
35 M. Matsumoto and T. Nishimura, *ACM Trans. Model. Comput. Simul.*, 1998, **8**, 3–30.
36 R. D. Groot and P. B. Warren, *J. Chem. Phys.*, 1997, **107**, 4423–4435.
37 M. Murat and G. Grest, *Macromolecules*, 1989, **22**, 4054–4059.
38 D. I. Dimitrov, A. Milchev and K. Binder, *J. Chem. Phys.*, 2006, **125**, 034905.
39 F. Lo Verso, S. A. Egorov, A. Milchev and K. Binder, *J. Chem. Phys.*, 2010, **133**, 184901.
40 F. Lo Verso, L. Yelash, S. A. Egorov and K. Binder, *J. Chem. Phys.*, 2011, **135**, 214902.
41 D. Deb, A. Winkler, M. H. Yamani, M. Oettel, P. Virnau and K. Binder, *J. Chem. Phys.*, 2011, **134**, 214706.
42 A. P. Kaushik and P. Clancy, *J. Chem. Phys.*, 2012, **136**, 114702.
43 M. K. Corbierre, N. S. Cameron and R. B. Lennox, *Langmuir*, 2004, **20**, 2867–2873.
44 Y. Habibi, I. Hoeger, S. S. Kelley and O. J. Rojas, *Langmuir*, 2010, **26**, 990–1001.
45 I. Hoeger, O. J. Rojas, K. Efimenko, O. D. Velev and S. S. Kelley, *Soft Matter*, 2011, **7**, 1957–1967.
46 L. Csoka, I. C. Hoeger, P. Peralta, I. Peszlen and O. J. Rojas, *J. Colloid Interface Sci.*, 2011, **363**, 206–212.
47 L. Csoka, I. C. Hoeger, O. J. Rojas, I. Peszlen, J. J. Pawlak and P. N. Peralta, *ACS Macro Lett.*, 2012, **1**, 867–870.
48 A. R. Lokanathan, A. Nykänen, J. Seitsonen, L.-S. Johansson, J. Campbell, O. J. Rojas, O. Ikkala and J. Laine, *Biomacromolecules*, 2013, **14**(8), 2807–2813.